Front velocity in models with quadratic autocatalysis

Vladimir K. Vanag[a] and Irving R. Epstein
Department of Chemistry and Volen Center for Complex Systems, Brandeis University, Waltham, Massachusetts 02454-9110

(Received 8 July 2002; accepted 13 August 2002)

Front propagation is studied in several reaction–diffusion models based on the Oregonator model of the Belousov–Zhabotinsky reaction. Each system involves autocatalysis ($X \rightarrow 2X$), termination ($2X \rightarrow 0$) and consumption of the autocatalyst ($X \rightarrow 0$, $X+Y \rightarrow 0$), augmented with interconversion ($X \leftrightarrow R$) between the autocatalyst *X* and a rapidly diffusing unreactive species R. We investigate the dependence of the front velocity on the diffusion coefficients of X and R, the interconversion rates, and the other kinetic parameters, when the system possesses either one or two stable steady states.
 [DOI: 10.1063/1.1511728]

I. INTRODUCTION

Recent discoveries of standing waves, accelerating waves, antispirals, and packet waves in the Belousov–Zhabotinsky (BZ) reaction dispersed in aqueous nanodroplets of water-in-oil Aerosol OT microemulsion (BZ–AOT system)[1–3] call attention to the need for deeper understanding and analysis of this system, one of whose most significant features is the presence of species which can diffuse at very different rates. A simple model of the BZ–AOT system[1] accounts for many of the experimentally observed phenomena. The model is obtained by augmenting the well-known Oregonator model (O1)–(O5) of the BZ reaction[4] with two new reactions (O6) and (O7).

$A+Y \rightarrow X$	k_1	(O1)
$X+Y \rightarrow P$	k_2	(O2)
$A+X \rightarrow 2X+2Z$	k_3	(O3)
$2X \rightarrow P$	k_4	(O4)
$B+Z \rightarrow hY$	k_5	(O5)
$X \rightarrow R$	k_f'	(O6)
$R \rightarrow X$	k_b'	(O7)

where $A=BrO_3^-$, $X=HBrO_2$, $Y=Br^-$, Z is the oxidized form of the catalyst, B is the sum of malonic and bromomalonic acids, R is $BrO_2^{\cdot}$ radical (or Br_2O_4) in the oil phase, and P represents unreactive products. The overall forward reaction (O6) consists of production of R in a water droplet $[HBrO_2+HBrO_3 \rightarrow 2BrO_2^{\cdot}$ (or $Br_2O_4)+H_2O]$ followed by interfacial transfer of the product from the droplet to the oil phase through the surfactant shell. The overall back reaction (O7) involves interfacial transfer from the oil phase into a droplet and then reaction of R with the reduced form of the catalyst, Cat ($Br_2O_4 \rightarrow 2BrO_2^{\cdot}$, $BrO_2^{\cdot}+Cat \rightarrow HBrO_2$), inside (or at the interface of) the droplet. In most studies of the Oregonator, the concentrations of A and B are taken to be constant, and X, Y, and Z serve as the variables.

The diffusion coefficients of the water-soluble species (X, Y, Z, A, and B) are equal to the diffusion coefficient (10^{-8}–10^{-7} cm^2/s) of entire droplets or clusters of droplets, while the diffusion coefficient of the oil-soluble species (R) is about 10^{-5} cm^2/s.[5] The very different diffusion coefficients of X and R, D_X and D_R, respectively, raise the question of how the velocity of reaction–diffusion waves in the BZ–AOT system depends on these parameters. For the Oregonator model (O1)–(O5), the wave velocity *c* is essentially determined by the rate of the autocatalytic step (O3) and is given by the Fisher–Kolmogorov equation[6,7] for the minimum velocity, c_{min}, of a propagating front with quadratic autocatalysis (see also Ref. 8)

$$c_{min}=2(D_X k_3[A])^{1/2}. \tag{1}$$

In the full system (O1)–(O7), we have the additional species R with a diffusion coefficient D_R much larger than D_X. What effect does the presence of this species have on the velocity of front propagation?

This problem has implications beyond the BZ–AOT system. Therefore we reformulate it more generally. A species X is formed autocatalytically. There are reactions in which this autocatalyst is consumed. Another form of the autocatalytic species, R, is unreactive, i.e., R does not take part in any reactions other than interconversion with X. R can diffuse much more rapidly than X. A biological analog is the production by organisms such as mushrooms, bacteria or plants of inactive forms, e.g., spores or seeds, which can be rapidly spread by the wind. We have not found in the literature, including a recent comprehensive review on chemical waves,[9] a treatment of the generic behavior of systems with fast inactive and slow active forms of the autocatalyst or activator species.

In this paper we analyze how front propagation depends on k_f' and k_b', which characterize the transformation between the reactive and unreactive forms of the autocatalyst, as well as on the other parameters of system (O1)–(O7). To focus the problem more clearly, we neglect for the moment the dynamics of Y, i.e., step (O5), which is responsible for the negative feedback in the BZ system, and step (O1), in which Y acts to generate X. We take [Y] in step (O2), the decay reaction, to be constant. Under these assumptions, we obtain the following scheme:

[a]Permanent address: Center for Photochemistry, Russian Academy of Sciences, Novatorov str., 7A, 117421, Moscow, Russia.

$$X \rightarrow 2X \qquad k_a \qquad (O3')$$
$$2X \rightarrow P_1 \qquad k_4 \qquad (O4')$$
$$X \rightarrow P_2 \qquad k_d' \qquad (O2')$$
$$X \rightarrow R \qquad k_f' \qquad (O6)$$
$$R \rightarrow X \qquad k_b' \qquad (O7)$$

with corresponding equations for front propagation in the case of quadratic autocatalysis with "slow" X and "fast" R species:

$$\partial[R]/\partial t = k_f'[X] - k_b'[R] + D_R \Delta[R], \tag{2}$$

$$\partial[X]/\partial t = k_a[X] - k_t[X]^2 - k_d'[X] - k_f'[X] + k_b'[R] + D_X \Delta[X], \tag{3}$$

where $k_a = k_3[A]$ is the effective rate constant of autocatalysis, $k_t = 2k_4$ is the termination constant, and $k_d' = k_2[Y]$ is the effective decay rate constant, $k_d' < k_a$. In one spatial dimension, the Laplacian Δ is $\partial^2/\partial\rho'^2$, where ρ' is the coordinate along the direction of front propagation. The system (2), (3) has one unstable steady state, $[X]_1 = [R]_1 = 0$, and one stable steady state, $[X]_3 = (k_a - k_d')/k_t$, $[R]_3 = k_f'[X]_3/k_b$ ($[X]_2$ will appear later). This system is an intriguing one, because it gives rise to a large average displacement of $R(\cong (D_R t)^{1/2})$ and a small shift of the X-front $(\cong t(D_X k_a)^{1/2})$ for times $t \ll D_R/(D_X k_a)$ that significantly exceed the characteristic time of autocatalysis, k_a^{-1}. Transition of R into X far beyond the front and the possibility of autocatalytic growth of X for small initial values of X may lead to a significant increase in the velocity of the propagating front, which transforms $[X]_1$ into $[X]_3$, above the value predicted by Eq. (1). We analyze this problem in Sec. II.

Another model, which is more faithful to the Oregonator, takes into account the effects of the negative feedback by introducing an additional term, $-k_{out}[X]/(K_m + [X])$, replacing Eq. (3) by Eq. (4),

$$\partial[X]/\partial t = k_a[X] - k_t[X]^2 - k_d'[X] - k_{out}[X]/([X] + K_m) - k_f'[X] + k_b'[R] + D_X \Delta[X]. \tag{4}$$

This modification transforms the unstable steady state $[X]_1 = 0$ into a stable steady state $[X]_1 = 0$ and an unstable steady state $[X]_2$. The resulting bistable system (2), (4) is analyzed in Sec. III.

Finally, by making the steady state approximation, $d[Y]/dt = 0$, we obtain $[Y] = (k_{out}/k_2)/([X] + K_m)$, where $k_{out} = hk_5[B][Z]$, and $K_m = k_1[A]/k_2$. Using this expression and including all steps in the Oregonator model (O1)–(O7), we have

$$\partial[X]/\partial t = k_a[X] - k_t[X]^2 - k_{out}([X] - K_m)/([X] + K_m) - k_f'[X] + k_b'[R] + D_X \Delta[X]. \tag{5}$$

The system (2), (5) is also bistable, but with nonzero stable steady states $[X]_1$ and $[X]_3$. It, too, is studied in Sec. III.

System (2), (3) corresponds to the so-called "pulled case" of front propagation in the classification suggested by Ben-Jacob[10] and employed in subsequent publications.[11–14] In this case, the front propagates into an unstable steady state $[[X]_{SS} = [R]_{SS} = 0$ for Eqs. (2), (3)], and any velocity ν greater than or equal to a minimum value ν_{min} yields a solution to the corresponding differential equations. The simplest one-variable example of front propagation, described by the following general equation:

$$\partial[X]/\partial t = F([X]) + \Delta[X], \tag{AW}$$

where $dF([X])/d[X] \equiv F'([X]) = 1$ at $[X] = 0$, was studied by Aronson and Weinberger.[15] They showed that the front velocity asymptotically approaches the value $\nu_{min} = 2$ [more exactly, $\nu_{min} = 2(F'(0))^{1/2}$] for a localized initial perturbation of the unstable steady state.

Based on a "linear marginal stability" hypothesis, Dee and Langer[16] and then van Saarloos[12,13] showed how the front velocity ν_{min} can be found for more complex (usually one-variable) equations, as long as the front still propagates into an unstable steady state. The "marginally stable" velocity ν_{min} has the property that all fronts with velocity $\nu > \nu_{min}$ are stable to perturbations, but fronts with $\nu < \nu_{min}$ are unstable.

Systems (2), (4) and (2), (5) belong to the "pushed case," [11] in which the propagating front switches one stable state to another (an unstable steady state lies between the two). For this case, simple linear stability analysis is insufficient.[17] We will compare our computer simulations with linear stability analysis for both cases.

II. SYSTEM WITH A SINGLE STABLE STEADY STATE

A. Linear stability analysis

If there is no interconversion of autocatalyst, $k_f' = k_b' = 0$, then the velocity of front propagation for Eq. (3) is[8]

$$c = c_{min}(1 - k_d'/k_a)^{1/2}, \tag{6}$$

where c_{min} is given by Eq. (1). For the two-variable system (2), (3), the front velocity, ν, may be found by linear stability analysis[8,18,19] of the steady state solutions of the ordinary differential equations obtained by introducing the moving coordinate $\eta = \rho - \nu t$.

First, we rewrite Eqs. (2), (3) in dimensionless form, substituting new variables $\tau = k_a t$, $x = (k_t/k_a)[X]$, $r = (k_t/k_a)[R]$, and $\rho = (k_a/D_X)^{1/2}\rho'$,

$$\partial x/\partial\tau = f(x) - k_f x + k_b r + \Delta x, \tag{7}$$

$$\partial r/\partial\tau = k_f x - k_b r + d\Delta r, \tag{8}$$

where $f(x) = (1 - k_d)x - x^2$, $k_f = k_f'/k_a$, $k_b = k_b'/k_a$, $k_d = k_d'/k_a$, $d = D_R/D_X$, $\Delta = \partial^2/\partial\rho^2$. In this dimensionless notation, $c_{min} = 2$.

The linear stability analysis of (7), (8), which involves converting the two partial differential equations to four first-order ordinary differential equations by first introducing the moving frame $\eta = \rho - \nu t$ and then defining variables equal to the η derivatives of the concentrations, is identical to that found in Ref. 19 and gives the following characteristic equation:

$$g(\lambda, \nu) \equiv \lambda^4 + \lambda^3\nu(1 + 1/d) + \lambda^2(df(x)/dx - k_f + \nu^2/d - k_b/d) - \lambda(\nu/d)(k_b + k_f - df(x)/dx) - (k_b/d)df(x)/dx = 0. \tag{9}$$

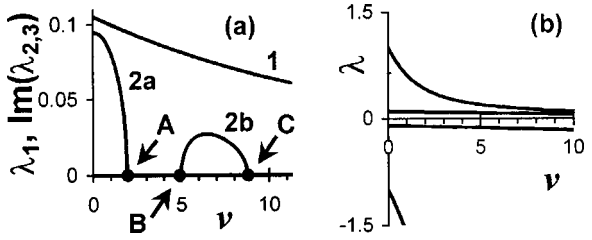

FIG. 1. Typical dependence of eigenvalues of Eq. (9) on front velocity ν. Parameters $d=100$, $k_f=0.1$, $k_b=1$, $k_d=0$. (a) Behavior of positive eigenvalue λ_1 (curve 1) and imaginary part of complex eigenvalue $\lambda_{2,3}$ [curves 2a (Im($\lambda_{2,3}$)/10) and 2b] for the steady state $x_{ss}^{(1)}=0$. At $k_f=1$, points *A* and *B* merge at $\nu=0$, and only point *C* remains [see Fig. 2(a)]. (b) Eigenvalues for the steady state $x_{ss}^{(3)}=(1-k_d)$.

The system has two steady states, $x_{ss}^{(1)}=0$ and $x_{ss}^{(3)}=(1-k_d)$, corresponding, respectively to the steady states $[X]_1$ and $[X]_3$ of Eqs. (2), (3). State $x_{ss}^{(1)}$, on which we focus, gives exactly one positive (λ_1) and one negative eigenvalue for all values of the parameters.[19] The other two eigenvalues may be either complex or real. The second steady state $x_{ss}^{(3)}=(1-k_d)$ gives four real eigenvalues, two negative and two positive [Fig. 1(b)].

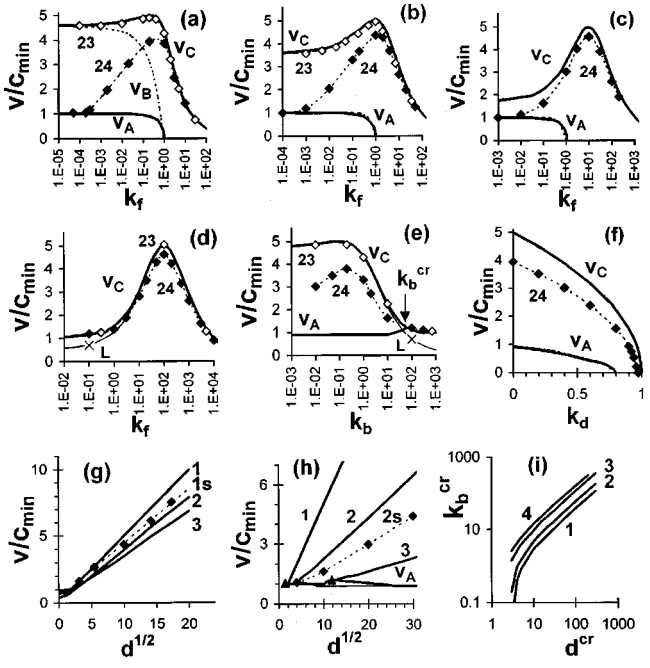

FIG. 2. Dependence of velocity of front propagation ν on parameters k_f, k_b, k_d, and d for systems (2), (3) and (2), (4). Bold lines are velocities ν_A and ν_C at points *A* and *C*, respectively [shown in Fig. 1(a)] obtained for system (2), (3). Solid lines "*L*" in (d) and (e) are velocity ν_C for system (2), (3) at $D_X=0$. Dashed lines without symbols (which nearly coincide with bold lines) are velocities ν_A and ν_C for system (2), (4) at small $K_m(=10^{-4})$ and $k_{out}(=0.01)$; dashed line ν_B in (a) shows velocity ν_B at point *B* in Fig. 1(a). All lines without symbols (e.g., ν_A, ν_B, and ν_C) are obtained by linear stability analysis. Velocities obtained by computer simulation of PDE (2), (3) and (2), (4) at $K_m=0.01$, $k_{out}=0.02$ (identical results are obtained at $K_m=10^{-4}$, $k_{out}=0.01$), are shown as "23" and "24" by open diamonds and filled diamonds [or triangles in (h)], respectively. Open diamonds are not connected by line but lie on curves ν_C. Cross ($\times$) in (d) and (e) marks velocity ν obtained by solution of PDE (2), (3) at $D_X=0$. (i) Dependence of k_b^{cr} on d^{cr} for $k_f<1$, where k_b^{cr} is shown by arrow in (e). Parameters are given in Table I.

TABLE I. Parameters k_f, k_b, k_d, and d of models (2), (3) and (2), (4) used in Fig. 2.

Parts and curves	k_f	k_b	k_d	d
a	var[a]	0.2	0	100
b	var	1	0	100
c	var	10	0	100
d	var	100	0	100
e	0.1	var	0	100
f	0.2	0.2	var	100
g1, g1s	1	1	0	var
g2	1	0.1	0	var
g3	1	10	0	var
h1	0.1	0.1	0	var
h2, h2s	0.1	10	0	var
h3	0.1	100	0	var
i1	0.01	var	0	var
i2	0.1	var	0	var
i3	0.5	var	0	var
i4	0.9	var	0	var

[a]var=variable.

If Eq. (9) were to possess a pair of complex eigenvalues for $x_{ss}^{(1)}$, the system would oscillate around $x_{ss}^{(1)}=0$, which would result in negative concentrations, which is physically impossible. The values of ν at which complex eigenvalues emerge [points *A*, *B*, and *C*, corresponding to velocities ν_A, ν_B, and ν_C in Fig. 1(a)] are therefore of special interest, since they allow us to determine the physically allowed range for the velocity of front propagation. The physically meaningful values of ν, where all eigenvalues λ are real (and all but λ_1 are negative), fall between points *A* and *B* or to the right of point *C* in Fig. 1(a).

The variation of ν_A and ν_C with some of the system parameters is shown as the bold lines in Fig. 2 (Table I). We see that when $k_f<1$ [actually, when $k_f+k_d<1$, see Fig. 2(f)] and $k_b<d/2$ [$k_b'<k_a d/2$, see Figs. 2(e) and 2(h)], the velocities ν_A and ν_C coexist. The smaller k_b, the more pronounced the difference between ν_A and ν_C. At higher values of k_f (when $k_f>1$), points *A* and *B* coincide with the origin in Fig. 1(a), and all values of ν less than ν_C give complex eigenvalues. The slower velocity ν_A is very close to c/c_{min} in Eq. (6) with k_d'/k_a replaced by k_d+k_f, i.e., ν_A is proportional to $D_X^{1/2}$. The faster velocity ν_C attains its maximum, ν_{max}, at $k_f=k_b$. More detailed analysis reveals that

$$\nu_{max}\cong c_{min}d^{1/2}/2. \tag{10}$$

Figures 2(g) and 2(h) show that ν_C/c_{min} is proportional to $d^{1/2}$ (i.e., ν_C is proportional to $D_R^{1/2}$) at $k_b<d/2$, but with a coefficient of proportionality that depends on k_f and k_b. For example, these coefficients are 0.496, 0.391, and 0.315 for curves 1, 2, and 3, respectively, in Fig. 2(g) (when $k_f=1$), and 0.495, 0.21, and 0.068 for curves 1, 2, and 3, respectively, in Fig. 2(h) (when $k_f=0.1$). Figure 2(f) demonstrates that ν_C and ν_A depend on k_d as $\nu_C=\nu_{0C}(1-k_d)^{1/2}$ and $\nu_A=\nu_{0A}(1-k_f-k_d)^{1/2}$, where ν_{0C} and ν_{0A} are equal to ν_C and ν_A, respectively, at $k_d=0$. These relationships are analogous to Eq. (6) and have a simple explanation. For quadratic autocatalysis, the front velocity is proportional to $(Dk_{auto})^{1/2}$ [see Eq. (1)], where D is the relevant diffusion coefficient

and k_{auto} is the effective pseudo-first-order rate constant for autocatalysis. Velocities ν_C and ν_A may be written as $\nu_C = \text{constant} \times [D_R h(k_f,k_b)(1-k_d)]^{1/2}$ and $\nu_A = \text{constant} \times [D_X(1-k_f-k_d)]^{1/2}$, where $h(k_f,k_b)$ is some function of k_f and k_b. The dependence of ν_C on k_f is more complex than that of ν_A [see Figs. 2(a)–2(d)]. For $k_f < k_b$, ν_C [i.e., $h(k_f,k_b)$] increases with k_f. When $k_f > k_b$, ν_C begins to decrease, and for $k_f \gg k_b$, ν_C varies as $k_f^{-1/2}$ [$h(k_f,k_b) = \text{constant} \times (k_f/k_b)^{-1/2}$]. In contrast, ν_A always varies with k_f and k_d as $(1-k_f-k_d)^{1/2}$, because reactions $X \to 0$ and $X \to R$ play the same decay role for X.

If we define k_b^{cr} and d^{cr} as the values at which ν_C and ν_A merge [see Figs. 2(e) and 2(h)], we find that $k_b^{\text{cr}} = c(k_f)d^{\text{cr}}$, as shown in Fig. 2(i), where for large d ($d > 10$), $c(k_f)$ is of order 1 and depends only on k_f; for example, $c(k_f) = 0.4$, 0.6, 1.2, 1.5, 1.6 at $k_f = 0.01$, 0.1, 0.5, 0.8, 0.9, respectively. For $k_f > 1$ or $k_b > c(k_f)d$ [i.e., $k_b' > k_a c(k_f) d$], linear stability analysis gives only a single velocity of front propagation.

The limiting case of Eqs. (2) and (3) when $D_X = 0$, which is formally equivalent to $d = \infty$ in Eqs. (7) and (8), provides some insight into the significance of ν_c. The analysis,[19] which is similar to that of Eqs. (7) and (8) (though here we have only three coupled first-order equations to deal with), gives the following characteristic equation:

$$\lambda^3 + \lambda^2(\nu + (1-k_d-k_f)/\nu) + \lambda(1-k_d-k_f-k_b) - k_b(1-k_d)/\nu = 0. \tag{11}$$

Again, one eigenvalue, λ_1, is always positive, and its dependence on ν resembles curve 1 in Fig. 1(a); i.e., λ_1 monotonically decreases with ν. Now, however, curve 2a is absent, and complex eigenvalues appear only between the analogs of points ν_C and ν_B (which we designate ν_{CL} and ν_{BL}, respectively). When $k_f < 1$, the imaginary part of the complex eigenvalues looks like curve 2b in Fig. 1(a), while for $k_f > 1$, only point ν_{CL} is present, i.e., a pair of complex eigenvalues exists for all $\nu < \nu_{CL}$. Numerical solution reveals that ν_{CL} and ν_{BL} coincide with ν_C and ν_B, except when ν_A is close to ν_C.[20] We see in Figs. 2(d) and 2(e) that ν_{CL} (curves L) is smaller than ν_C and ν_A at small k_f ($k_f < 1$) [Fig. 2(d)] and large k_b ($k_b > d/2$) [Fig. 2(e)]. In the limit of $k_f \to 0$ or $k_b \to \infty$, the front velocity vanishes for $D_X = 0$; it equals ν_A (or $c_{\min}$) for positive D_X. We conclude that the velocity ν_C found by linear stability analysis of system (2) and (3) is the front velocity for the limiting case $D_X = 0$ and depends only on D_R; i.e., when $D_X = 0$ the front is "carried by" the species R.

B. Computer simulations

In addition to the linear stability analysis, we also integrated the partial differential equations (PDE) (7) and (8) using FlexPDE,[21] in which a Newton–Raphson iteration process is used with a variable time step and mesh. FlexPDE refines the triangular finite element mesh until the estimated error in any variable is less than a specified tolerance, which we chose as 10^{-6}, at every cell of the mesh. Calculations were performed on a quasi-one-dimensional rectangle of width 1 and length L, where $L = 100$, 200, or 400; the longer rectangles being used for broader fronts. The initial conditions were chosen as $[R]_0 = k_f[X]_0/k_b$, $[X]_0 = [X]_3$ at $0 < \rho < L/100$ and $[X]_0 = 0$ at all other points. No-flux boundary conditions or fixed-value boundary conditions with $[X] = [X]_3$, $[R] = k_f[X]_3/k_b$ were used at the left boundary and $[X] = [R] = 0$ at the right boundary (the front propagates from left to right). Using no-flux boundary conditions at both borders yields the same result, since the length L is large relative to the characteristic length scales of the system.

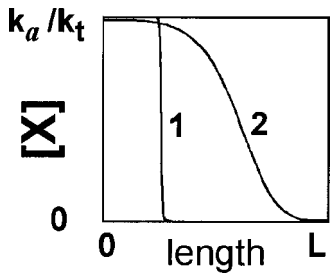

FIG. 3. Front profiles for stationary regimes of front propagation in system (2), (3). Parameters $k_a = 1$, $k_t = 0.01$, $k_d = 0$, $k_b = 1$, $L = 100$, $D_X = 0.01$, $D_R = 1$, $k_f = (1)$ 0, (2) 20.

At $k_f = 0$, the calculated front velocity coincides with the theoretical value, Eq. (1), and the front is quite sharp (Fig. 3, curve 1). The width of the front increases with k_f (Fig. 3, curve 2). Simulations of system (2) and (3) reveal that at any k_f and k_b the calculated velocities (open diamonds in Fig. 2) coincide with the theoretical values ν_C. Even at $k_f < 1$, when two velocities ν_A and ν_C coexist [see Figs. 2(a), 2(b), and 2(e)], the front velocity is equal to ν_C and depends on D_R rather than on D_X.

Calculations on system (2) and (3) at large d ($\cong 100$) and at $D_X = 0$ give nearly identical values of ν, except at small k_f and large k_b. Results for this case are shown in Figs. 2(d) and 2(e) by crosses, which lie on the theoretical curves L (ν_{CL}).

III. BISTABLE SYSTEMS

A. System (2), (4)

We first modify Eq. (3) by introducing the small additional term $k_{\text{out}}[X]/(K_m + [X])$ to produce Eq. (4). This term mimics reaction (O2) if we set $[Y] = (k_{\text{out}}/k_2)/(k_m + [X])$, but unlike the more complete Eq. (5), which includes the term arising from reaction (O1) and which we consider below, it maintains the steady state at $[X] = 0$. The significance of this state is that it allows one to invoke the argument that velocities leading to complex eigenvalues in the linear stability analysis are not physically meaningful, since the system cannot oscillate about a zero concentration. Coupled with the dependence of the positive eigenvalue λ_1 on ν, this situation allows us to employ linear stability analysis to select ν_A and ν_C as the stable velocities for wave propagation. We expect the wave front for system (2), (4) to have the same dependence on the system parameters as the front in system (2), (3) as $k_{\text{out}} \to 0$, except when the existence of a threshold concentration of [X], below which autocatalysis cannot start, becomes significant.

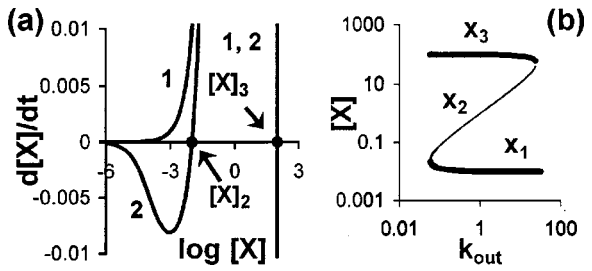

FIG. 4. (a) Dependence of $d[X]/dt$ on [X] for system (2), (3) (curve 1) and (2), (4) (curve 2). Parameters $k_a=1$, $k_t=0.01$, $k_d=0$, $K_m=10^{-4}$, and $k_{out}=10^{-2}$. (b) Dependence of stable steady states $[X]_1$ and $[X]_3$ and unstable steady state $[X]_2$ on k_{out} for system (2), (4) at $k_a=1$, $k_t=0.01$, $k_d=0$, and $K_m=0.01$.

1. Linear stability analysis

The effect on the steady states of adding this new term with relatively small k_{out} and K_m, and $k_{out}/(k_a-k_d')>K_m$ is shown in Fig. 4(a). The unstable steady state $[X]_1=0$ is transformed into a stable state $[X]_1=0$ and an unstable steady state $[X]_2$. Under these conditions, $[X]_2\cong k_{out}/(k_a-k_d')-K_m$. The difference between $[X]_2$ and $[X]_1$ is the threshold concentration of [X]. In the calculations below, we take $k_a=1$, so we can replace k_f' by k_f, k_b' by k_b, k_d' by k_d, and τ by t.

We carried out a linear stability analysis of system (2), (4) analogous to that performed for system (2), (3), but with $df(x)/dx=k_a-k_d-2k_t[X]_{SS}-k_{out}K_m/(K_m+[X]_{SS})^2$ in the characteristic Eq. (9). For the stable states $[X]_{SS}=[X]_1$ and $[X]_{SS}=[X]_3$ the dependence of the eigenvalues λ on ν resembles that shown in Fig. 1(b) in that all eigenvalues are real and vary monotonically with ν. For the unstable state $[X]_{SS}=[X]_2$, the behavior of the eigenvalues is analogous to that shown in Fig. 1(a), and the dependence of ν_A and ν_C on the parameters mirrors that shown in Fig. 2. For small k_{out} and very small K_m, when $k_{out}/K_m>100$, ν_A and ν_C depend on the parameters as they do in the monostable case. At small k_{out} and K_m, when k_{out}/K_m only slightly exceeds 1 (e.g., $k_{out}=0.02$, $K_m=0.01$), ν_A and ν_C show quantitative differences (e.g., ν_C decreases at $k_f<1$), but the qualitative behavior does not change. Although the steady state concentration $[X]_2$ is positive, and when λ is complex small amplitude oscillations around $[X]_2$ are possible in principle, $[X]_2\to[X]_1=0$ as $k_{out}\to 0$, and the velocities ν_A and ν_C may still give a good approximation to the actual velocity of the front, despite the fact that the argument regarding complex eigenvalues is applied here to the *nonzero* steady state $[X]_2$. We analyze this question numerically in the next section. To find exact expressions for the velocity of the front that connects two stable steady states, other mathematical methods may be applied,[8,9,14,17] which yield a discrete spectrum of possible velocities ν_{front}. These techniques (analogous to solution of the Schrödinger equation) are beyond the scope of the present paper.

2. Computer simulation

The quasi-one-dimensional partial differential equations (2), (4) were numerically integrated on a rectangle of length L and width 1 with initial conditions $[R]_0=k_f[X]_0/k_b$, $[X]_0>[X]_2$ for $0<\rho<L/100$ and $[X]_0<[X]_2$ at all other points. Zero-flux boundary conditions were used at the left boundary and $[X]=[R]=0$ at the right boundary (the front propagates from left to right).

The front velocity depends strongly on k_f and k_b. The simulated velocity ν (shown in Fig. 2 as "24," filled symbols) coincides with ν_C when $k_f>1$ ($k_f'>k_a$) or $k_b>c(k_f)d$, and, also in agreement with the results of linear stability analysis, $\nu_{max}\cong(D_R k_a)^{1/2}$ at $k_f=k_b$. However, when $k_f<1$ and $k_b<c(k_f)d$ [see Figs. 2(a), 2(b), and 2(e)], ν is significantly smaller than ν_C, lies between ν_A and ν_C, and $\nu\to c_{min}$ at very small k_f. This behavior differs dramatically from that found for system (2), (3). We conclude that the threshold $[X]_2-[X]_1$ plays a crucial role for small k_f and k_b [$k_f<k_b$, $k_f<1$, $k_b<c(k_f)d$] and that the velocity found by linear stability analysis of the unstable steady state $[X]_2$ is not a good approximation to the actual velocity. However, for large k_f or large k_b, this threshold is not important.

The inequality $k_f'>k_a$ ($k_f>1$) is similar to the condition $k_d'>k_a$. The forward interconversion reaction X→R and decay reaction X→0 both consume the autocatalyst, but differ in that the latter reaction is irreversible. The inequality $k_d'>k_a$ implies termination of autocatalysis and leads to a zero front velocity [propagation failure, see Eq. (6)]. The inequality $k_f'>k_a$ means that the autocatalytic species X is unable to serve as the front-propagating species, because its interconversion to R outpaces its autocatalytic production. Thus, the front propagation now depends critically upon the diffusion of R. Therefore, the calculated ν coincides with ν_C at $k_f>1$.

The inequality $k_b'>k_a c(k_f)d$ arises from the competition between the interconversion reaction R→X and the diffusion of X and R. The characteristic diffusion length for X may be estimated as $l_X=(D_X/k_a)^{1/2}$. The characteristic time for R to diffuse a distance l_X is l_X^2/D_R. This time may be compared with the characteristic time for transformation of R into X, $(k_b')^{-1}$. If $(k_b')^{-1}<l_X^2/D_R$ [which is equivalent, within a factor of order unity, to $k_b'>k_a c(k_f)d$], we have equilibrium between X and R. Under these conditions, linear stability analysis gives the correct results and the profile of [X] coincides with that of $k_b[R]/k_f$, while for small k_b' [$k_b'<k_a c(k_f)d$] and small k_f'($k_f'<k_a$), the equilibrium condition $k_f[X]=k_b[R]$ does not hold.

The dependence of ν on k_d [Fig. 2(f)] is well described by the expression $\nu=\nu_0(1-k_{ef}-k_d)^{1/2}$, where k_{ef} is a small constant that depends on K_m and k_{out}, and $\nu_0=\nu$ at $k_d=0$. Figures 2(g) and 2(h) demonstrate that ν is proportional to $d^{1/2}$, as predicted by linear stability analysis, for $k_b'/k_a<c(k_f)d$.

B. System (2), (5)

If we assume that [Z]=constant and make the steady state approximation with respect to Y in the full system (O1)–(O7),[22] we obtain system (2), (5) with $k_{out}=hk_5[B]\times[Z]$. System (2), (5) differs from system (2), (4) primarily in that the stable steady state $[X]_1$ now occurs at a nonzero concentration. We expect the dependence of ν on k_f, k_b, and d to resemble that shown in Fig. 2 for system (2), (4), if $[X]_2$

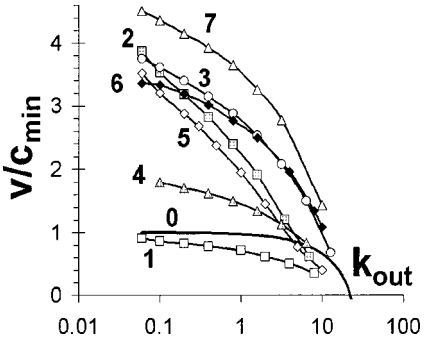

FIG. 5. Dependence of ν on k_{out} for system (2), (5). Parameters k_f and k_b are shown in Table II, $k_a=1$, $K_m=0.01$, $k_t=0.01$, $D_{\text{X}}=0.01$, $D_{\text{R}}=1$, $c_{\min}=2(k_aD_{\text{X}})^{1/2}=0.2$. Curve 5 represents two nearly identical curves for $k_f=0.2$ obtained with different values of k_b. Curve 0 is normalized velocity obtained from Eq. (14), where x_1, x_2, and x_3 are shown in Fig. 4(b).

is close to $[\text{X}]_1$. In this section, we focus on the dependence of ν on k_{out} and K_m, which determine the unstable steady state concentration $[\text{X}]_2$.

The steady states of this system are given by Eq. (12). The behavior for a typical set of parameters is shown in Fig. 4(b),

$$d[\text{X}]/dt=k_a[\text{X}]-k_t[\text{X}]^2-k_{\text{out}}([\text{X}]-K_m)/([\text{X}]+K_m)=0. \tag{12}$$

When $[\text{X}]_2$ and $[\text{X}]_3 \gg K_m$, they may be approximated as $[\text{X}]_{2,3}\cong 0.5(k_a\pm[k_a^2-4k_tk_{\text{out}}]^{1/2})/k_t$. When $[\text{X}]\ll k_a/k_t$, $[\text{X}]_1$ and $[\text{X}]_2$ are given by $[\text{X}]_{1,2}\cong 0.5(k_{\text{out}}/k_a-K_m \pm[(k_{\text{out}}/k_a-K_m)^2-4K_mk_{\text{out}}/k_a]^{1/2})$. Bistability can occur only when k_{out} lies between $k_{\text{out-min}}\cong K_m(3+8^{1/2})$ and $k_{\text{out-max}}\cong k_a^2/4k_t$. For this range of k_{out}, Eq. (12) may be written in the form

$$d[\text{X}]/dt=k_t([\text{X}]-[\text{X}]_1)([\text{X}]-[\text{X}]_2)\times([\text{X}]_3-[\text{X}])/([\text{X}]+K_m). \tag{13}$$

Note that for the one-variable system described by the cubic equation: $\partial x/\partial t=(x-x_1)(x-x_2)(x_3-x)+\partial^2x/\partial\rho^2$ (where $x_1<x_2<x_3$), the front velocity ν_{front} is given by (see, for example, Refs. 8 and 14)

$$\nu_{\text{front}}=(x_1+x_3-2x_2)/(2^{1/2}). \tag{14}$$

We studied the dependence of ν on k_{out} at a single value of K_m. Our results are summarized in Fig. 5 (Table II). Curve 1 in Fig. 5 is a reference curve for $k_f=k_b=0$ [and can be compared with Eq. (14), see curve 0 in Fig. 5]. In all cases, ν decreases with k_{out} or, equivalently, with the threshold for transition, $[\text{X}]_2-[\text{X}]_1$. The sensitivity of ν to changes in k_{out} (measured as $\partial\nu/\partial k_{\text{out}}$) depends on k_f and k_b. If k_f is less than 1, but not so small that the diffusivity of R makes no contribution to front propagation (curves 2 and 5), then $|\partial\nu/\partial k_{\text{out}}|$ is large at small k_{out}; when $k_f>1$ (curves 4 and 6), $|\partial\nu/\partial k_{\text{out}}|$ is small at small k_{out}. This behavior arises from the different modes of wave propagation at small and large k_f. When $k_f>1$ and $[\text{X}]_2$ is small (k_{out} is small), the velocity ν coincides with ν_C, which is determined primarily by the diffusion of R, for which there is essentially no threshold or barrier. When $k_f<1$, the contribution of ν_A or, more precisely, of the diffusion of X, to the total velocity ν is significant. Therefore the barrier to switching between states, $[\text{X}]_2-[\text{X}]_1$, which depends upon k_{out}, plays an important role. We obtain nearly identical results (curve 5) for $k_b=0.04$ or 1 with $k_f=0.2$, which suggests that the equilibrium constant k_f/k_b does not affect the dependence of ν on k_{out} (or on $[\text{X}]_2$). This conclusion is supported by the fact that curves 3, 5, and 6, all of which have $k_f/k_b=5$, show quite different behavior.

TABLE II. Parameters k_f and k_b for model (2), (5) used in Fig. 5.

Curve	k_f	k_b
1	0	0
2	0.2	0.2
3	1	0.2
4	5	0.2
5	0.2	1
5	0.2	0.04
6	5	1
7	100	100

IV. CONCLUSION

We have shown that introducing an inactive, rapidly diffusing form, R, of the activator species, X, causes significant changes in the propagation velocity given by the Fisher–Kolmogorov equation (1).

In general, the velocity of the propagating front depends on both diffusion coefficients D_{X} and D_{R}. If $k_f'>k_a$, the wave is "carried" largely by the rapidly diffusing species, and ν depends mainly on D_{R}. When $k_f'<k_a$ (and $k_f'\ll k_b'\ll dk_a$), only a small amount of the activator is transformed to R, and wave propagation should depend primarily on X and D_{X}. This is indeed the case for the bistable system (2), (4), but, for the monostable system (2), (3), which does not possess a threshold of [X] for initiating autocatalysis, the velocity still depends on D_{R}. Very small concentrations of X far beyond the main visible front can lead to autocatalysis and acceleration of the front in system (2), (3). The existence of a threshold $[\text{X}]_2-[\text{X}]_1$ in the bistable system (2), (4) wipes out this effect. The analogous result was obtained for discrete systems[19,23–25] and so-called "cutoff" fronts,[26] where a threshold was present.

For system (2), (4), at intermediate transformation rates ($k_f'<k_a$) and at $k_b'<k_ac(k_f)d$, the velocity lies between the limits ν_A and ν_C determined by the diffusion rates of pure X and pure R. We have not obtained analytical expressions for ν in this range of parameters, where linear stability analysis is not sufficient.

The velocity attains its maximum value when $k_f=k_b$, because the system is then able to balance the two "forces" that tend to drive the wave forward. If k_f is much larger than k_b, the system is depleted of the activator X, and the autocatalytic reaction slows down, much as occurs if the rate of the decay reaction increases [see Fig. 2(f)]. If, on the other hand, k_b is too large, $k_b'>k_ac(k_f)d$, not enough R is present, and the system cannot "take advantage" of that species' more rapid diffusion rate. If k_f and k_b exceed the character-

istic reaction and diffusion rates of the system $[k_f' > k_a, k_b' > k_a c(k_f) d]$, then X and R reach (pseudo)-equilibrium, and the results of linear stability analysis describe both systems (2), (3) and (2), (4) well.

Analysis of the full system (O1)–(O7) shows standing waves[1] only when $k_f' < k_a$ and $k_b' < k_a c(k_f) d$. It is an open question whether there is an inherent connection between the existence of two possible velocities ν_A and ν_C for traveling waves and the ability to support standing waves.

ACKNOWLEDGMENTS

The authors thank Lingfa Yang, Milos Dolnik, and Anatol M. Zhabotinsky for helpful discussions. This work was supported by the Chemistry Division of the National Science Foundation.

[1] V. K. Vanag and I. R. Epstein, Phys. Rev. Lett. **87**, 228301 (2001).
[2] V. K. Vanag and I. R. Epstein, Science **294**, 835 (2001).
[3] V. K. Vanag and I. R. Epstein, Phys. Rev. Lett. **88**, 088303 (2002).
[4] R. J. Field and R. M. Noyes, J. Chem. Phys. **60**, 1877 (1974).
[5] L. J. Schwartz, C. L. DeCiantis, S. Chapman, B. K. Kelley, and J. P. Hornak, Langmuir **15**, 5461 (1999).
[6] R. A. Fisher, Ann. Eugen. **7**, 355 (1937).
[7] A. N. Kolmogorov, I. G. Petrovski, and N. S. Piskunov, Bull. Moscow State Univ., Series A **1**, 1 (1937).
[8] P. Gray and S. K. Scott, *Chemical Oscillations and Instabilities: Nonlinear Chemical Kinetics* (Clarendon, Oxford University Press, Oxford, 1990).
[9] A. G. Merzhanov and E. N. Rumanov, Rev. Mod. Phys. **71**, 1173 (1999).
[10] E. Ben-Jacob, H. Brand, G. Dee, L. Kramer, and J. S. Langer, Physica D **14**, 348 (1985).
[11] G. C. Paquette, L.-Y. Chen, N. Goldenfeld, and Y. Oono, Phys. Rev. Lett. **72**, 76 (1994).
[12] W. van Saarloos, Phys. Rev. E **37**, 211 (1988).
[13] W. van Saarloos, Phys. Rev. E **39**, 6367 (1989).
[14] V. A. Vasilev, Ju. M. Romanovskii, D. S. Chernavskii, and V. G. Yakhno, *Autowave Processes in Kinetic Systems. Spatial and Temporal Self-Organization in Physics, Chemistry, Biology and Medicine* (Deutscher Verlag, Berlin, 1987).
[15] D. G. Aronson and H. F. Weinberger, in *Partial Differential Equations and Related Topics*, edited by A. Goldstein (Springer-Verlag, Berlin, 1975), pp. 5–49.
[16] G. Dee and J. S. Langer, Phys. Rev. Lett. **50**, 383 (1983).
[17] W. van Saarloos, Phys. Rep. **301**, 9 (1998).
[18] P. Gray, S. K. Scott, and K. Showalter, Philos. Trans. R. Soc. London, Ser. A **337**, 249 (1991).
[19] V. K. Vanag and I. R. Epstein (unpublished).
[20] Note that the maximum value of ν_{CL} is 1, at $k_f = k_b$. In Fig. 2 it appears that $\max(\nu_{CL}) = 5$, because, to compare ν_{CL} with $\nu_C / c_{\min}$, we present ν_{CL} as $\nu_{CL} / (4 D_X)^{1/2}$ with D_X set to 0.01, the value used for simulation of the full system (2), (3).
[21] FlexPDE, http://www.pdesolutions.com/flexpde.htm (2001).
[22] Making the steady state approximation with respect to Z, as opposed to treating [Z] as a parameter, yields a system that resembles (2), (3) in having two non-negative steady states, an unstable one at $[X] = 0$ and a stable one at positive $[X]_3$. This version of the model has an additional, unphysical steady state at negative [X].
[23] H. P. Breuer, W. Huber, and F. Petruccione, Physica D **73**, 259 (1994).
[24] J. Cook and B. Derrida, J. Stat. Phys. **61**, 961 (1990).
[25] B. Derrida and H. Spohn, J. Stat. Phys. **51**, 817 (1988).
[26] E. Brunet and B. Derrida, Phys. Rev. E **56**, 2597 (1997).